Lightweight, transparent piezoresistive sensors conceptualized as anisotropic magnetorheological elastomers: A durability study

Martin Cvek , Erika Kutalkova , Robert Moucka , Pavel Urbanek , Michal Sedlacik

PII: S0020-7403(20)30045-X
DOI: https://doi.org/10.1016/j.ijmecsci.2020.105816
Reference: MS 105816

To appear in: *International Journal of Mechanical Sciences*

Received date: 3 January 2020
Revised date: 20 May 2020
Accepted date: 23 May 2020

Please cite this article as: Martin Cvek , Erika Kutalkova , Robert Moucka , Pavel Urbanek , Michal Sedlacik , Lightweight, transparent piezoresistive sensors conceptualized as anisotropic magnetorheological elastomers: A durability study, *International Journal of Mechanical Sciences* (2020), doi: https://doi.org/10.1016/j.ijmecsci.2020.105816

Highlights

- ✓ *Piezoresistive sensors (PSs) based on magnetorheological elastomers are designed*
- ✓ *Said PSs are lightweight with excellent transparency and sensitivity to pressure*
- ✓ *Performance of the PSs is investigated before and after exposure to cyclic loading*
- ✓ *The procedure described represents a feasible means for fabricating the novel PSs*

Lightweight, transparent piezoresistive sensors conceptualized as anisotropic magnetorheological elastomers: A durability study

Martin Cvek, Erika Kutalkova, Robert Moucka, Pavel Urbanek, Michal Sedlacik *

Centre of Polymer Systems, University Institute, Tomas Bata University in Zlín, Trida T. Bati 5678, 760 01 Zlín, Czech Republic

**Author to whom correspondence should be addressed: msedlacik@utb.cz*

Abstract. *Conductive elastic composites currently dominate in research efforts on soft electronics, such as wearable and flexible sensors. Typically, the conductivity of polymeric bodies is ensured by the incorporation of fillers. Using this approach, the weight of the composite is undesirably increased and optical properties such as transparency are entirely lost; both of these factors restrict the breadth of potential applications. Herein, we report on the development of lightweight, yet transparent, piezoresistive sensors. In order to obtain the percolating systems, the filler particles were organized using the external magnetic field into chain-like structures that acted as transport pathways for electric charge. The effect of particle concentration (1 to 7 wt.%) on piezoresistivity was investigated on custom-built apparatus. In line with rise in concentration, only a slight increment in structural density was observed (ca 6.5%), although notably there was more than a 100-fold increase in conductivity. The transparency in the direction of the particle chains was preserved to a great extent. The fatigue test revealed that conductivity inevitably diminished with compression loading cycles. Thorough discussion is given to options for extending the service life of such sensors.*

Keywords: *piezoresistivity; mechanical testing; electrical properties; polymer-matrix composites; magnetorheological elastomer*

1. Introduction

A piezoresistive sensor (PS) is a device that detects exerted force and translates it into a change in electrical resistivity upon deformation. Unlike piezoelectric sensors, PSs require

power from an external voltage source [1, 2]. Numerous applications for PSs have been found in robotics, electronics and sensing technology [3-5]. The most popular material for fabricating PSs is silicone. The physical principle behind the mechanism for silicone-based PSs is manifested at an atomic level, founded on change in band gap upon application of mechanical stress [2]. Apart from silicone, other elastic semiconductor bodies, such as germanium and gallium arsenide, can be used to construct PSs. However, this group of materials suffers from a lack of flexibility, making them unsuitable for certain applications, such as flexible electronics [6]. It is possible to eliminate this drawback by using polymer-based PSs instead [1, 6].

Polymer-based PSs are composites that comprise a polymeric matrix supplemented with conductive fillers. Various materials have been utilized as the basis, including polydimethylsiloxane (PDMS) [4, 6], poly(methyl methacrylate) [3], polycarbonate [5] and polyethylenimine [7]. Conductivity is ensured by employing carbon nanotubes [3, 5], graphene [6] or carbon black [4]. In contrast to traditional semiconductors, the advantages of polymer-based PSs are flexibility, low cost and, often, biocompatibility, all of which are favourable when it comes to wearable electronics [1, 6].

Besides electrically conductive, non-magnetic, particulate fillers (as mentioned above), magnetic fillers have been successfully applied in the development of sensors [8]. Embedding magnetic particles into the elastomeric matrix brings about the potential to obtain systems conceptually identical to magnetorheological elastomers (MREs) [9]. MREs are predominantly used in vibration absorption and adaptive damping, as they have a capacity for field-controlled hardening, otherwise known as the magnetorheological effect [10, 11]. They also demonstrate other features, including magnetostriction [9, 11], piezoresistance [8], magnetoresistance [8, 12] and even change in surface roughness [13], aspects currently under investigation within contemporary research and development. All these phenomena are closely related to externally induced changes in particle position,

giving rise to variation in the properties of the MRE material, with electrical conductivity being of particular interest for sensing applications.

The electrical conductivity of the MREs follows the standard percolation theory [1]. Typically, at low concentrations, metal particles are isolated and randomly distributed in the polymer matrix, while the MRE itself possesses extremely low conductivity (below 10^{-12} S/cm). Raising the concentration of particles means that they become closer to one another, and once an electrically conductive path is established, a dramatic jump in electrical conductivity (over several orders of magnitude) is achieved [14]. The critical concentration of filler at which the conductive path is formed is known as the percolation threshold (PT). Its value is dictated by certain physicochemical parameters of the fillers (surface area, roughness, aspect ratio) as well as the matrix, including conditions pertaining to how the composite is prepared [15, 16].

It has been found [14] that isotropic MREs with the embedded carbonyl iron (CI) particles, as the most popular dispersed phase in magnetorheology, percolate at concentrations between 10–15 vol.%. The fact is, though, that common concentrations in such MREs for sensing applications far exceed this limited range [8, 16, 17], making the resultant composites too heavy, uneconomical to produce and less flexible. Admittedly, a large content of CI particles in combination with high conductivity are essential factors for specific applications, such as sensors which simultaneously detect mechanical and magnetic signals [18]. In spite of this, standard practice would appear to be co-embedding highly conductive fillers rather than raising CI content, the aim being to increase conductivity and shift the PT value of isotropic MRE-based PSs. In this context, Bica et al.[8] incorporated graphene into an isotropic MRE to boost conductivity, and stabilized its time response for very short time intervals. The same authors have also experimented with graphite additives [12]. Shabdin et al.[19] have recently expanded knowledge on the topic by directly correlating the magnetorheological and resistivity properties of such a composite.

It is supposed that in applications requiring the dual qualities of high electrical conductivity and light weight, anisotropic MREs are preferred over their isotropic analogues. Anisotropy is achieved by exposing the mixture of magnetic particles and liquid-state matrix to a unidirectional magnetic field prior to the curing process. The first mention of anisotropic MREs dates back to an early paper (1999) by Ginder et al.[20], wherein it was revealed that the inherent microstructure significantly affected subsequent macroscopic properties, indicating previously untapped potential, a finding which rapidly spread throughout the research community. Later on, Li et al.[21] found that field-induced structures in an anisotropic MRE enhanced dynamic stiffness and damping properties. In addition to mechanical properties, structural configuration was seen to alter the shape of the magnetization curve for such an MRE [22]. Other manuscripts highlighted that particle alignment incremented dielectric response [23] and thermal conductivity [24] along conducting paths. To be rigorous, it should be emphasized that a composite with virtually the same microstructure as an anisotropic MRE had been developed even earlier (1992) by Jin et al.[25], who devised an optically transparent, yet electrically conductive composite medium. Their silicone-based system contained a small fraction of oriented Ni micro-spheres, a material which ensured high conductivity but still transmitted over 90% of incidental light.

While the conductivity of isotropic MREs adheres to a standard percolation dependence, their anisotropic analogues exhibit much higher conductivities (above 10^{-7} S/cm) even at reduced particle concentrations, causing loss in total weight [14]. This combination of properties marks them out for possible application in sophisticated electronic devices, e.g. sensors or alarms for pressure-sensitive controllers. The anticipated lifespan of these cyclically loaded assemblies is of great importance to practical usage. To date, very few studies have been devoted to in-depth investigation of the related phenomena of MRE-based composites. Zhang et al.[26] examined the effects of cyclic loading and thermal ageing on

the magnetorheological and mechanical behaviour of conventional MREs. Said authors reported fatigue-induced decrease in the storage modulus accompanied by amplification of the magnetorheological effect, explained by destruction of the particle aggregates, giving rise to better particle dispersion. The topic was later extended by Wang et al.[27], who showed the implications of cyclic loading on the electrical performance of densely filled isotropic MREs. Different conclusions were reported for MREs packed with electro-conductive carbon black, in which the magnetorheological effect did not interfere with the fatigue-induced rise in resistance [28]. All these papers dealt merely with opaque materials carrying high amount of metal particles, the most expensive components integrated in the PSs. In order to address this limitation and cut the cost of the final products, we developed a novel concept that allowed for restriction in weight of the PSs, while still preserving their flexibility and high unidirectional transparency.

Herein, the lightweight polymer-based PSs conceptualized as anisotropic MREs were fabricated from a PDMS matrix and filled with an extremely low content of CI particles (less than 1 vol.%), thereby enabling transparency, an aspect absent from previous studies. The effect of particle concentration on conductivity and resistance was studied under defined pressure loadings to characterize the stimulus sensitivity of the PSs. From the viewpoint of practical application, the PSs were further subjected to cyclic loading that simulated real-world conditions. Investigation was made as to post-loading phenomena occurring at the particle/matrix interphase, such as particle debonding or irreversible matrix deformation, and their effects on piezoresistivity were re-examined and compared with the initial state. Finally, options were evaluated for extending the service life of the PSs, and consideration was given to future challenges.

2. Experimental

2.1 Fabrication of the MRE-based PSs. Several techniques can be employed to fabricate polymeric smart elements, including hot pressing [29], injection moulding [10], depositing

on substrates [8], formation of sandwich structures [30], rapid prototyping and 4D printing [31]. Herein, we applied the casting method and opted for a liquid-state polymer blend for the sake of simplicity, as no special manufacturing devices were needed. CI particles (SL grade, d_{50} = 9 µm); BASF, Germany) were used as the magnetic filler for the MRE-based PSs. Polydimethylsiloxane elastomer and the corresponding curing agent (Sylgard® 184, Dow Chemical Company, USA) served as the matrix. The weight ratio of the PDMS components was 10:1, as recommended by the supplier. The MRE-based PSs were prepared with various concentrations of the CI, namely 1, 3, 5 and 7 wt.%, while neat PDMS acted as a reference (further coded as: PS_particle concentration in wt.%). A calculated amount of the CI was mixed with the dual-component silicone elastomer on a high-speed vacuum mixing unit (Twister venturi, Renfert, Germany). Stirring was performed at laboratory temperature at 350 rpm for 10 min. until a homogeneous state was achieved. Any trapped air bubbles were removed from the mixtures in a vacuum chamber set to 10 mbar at laboratory temperature for 5 min. Subsequently, the mixture was cast in a cylindrical mould with a height of 4 mm and diameter of 30 mm. The mould was placed between the poles of a custom-built electromagnet in a heat chamber. A homogeneous static magnetic field of 340 mT was applied to the liquid-state sample during the polymerization process, which occurred at 80 °C for 3 hrs. The magnetic field in the mould was verified by a teslameter (Magnet-Physik, FH 51, Dr Steingroever, Germany). After the polymerization process had ended, the samples were left to cool down to laboratory temperature. Figure 1 shows a macroscopic view of the fabricated MRE-based PSs.

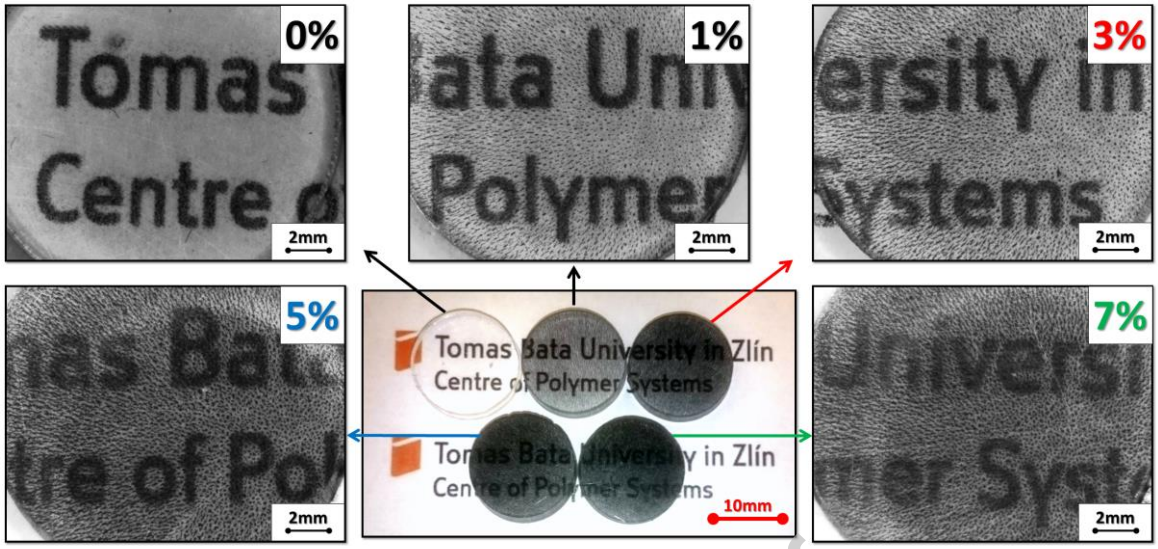

Fig. 1: Digital photograph of the MRE-based PSs with different concentrations of CI (centre) and magnified views (as per the corresponding arrows); the central image shows that the samples are transparent when placed on a flat surface; the thickness of the samples is 4.01±0.10 mm.

2.2 Piezoresistivity tests. Piezoresistivity experiments were conducted on an electrometer (Keithley 6517A, USA) coupled with a tensile machine (M350-5CT, Testometric, UK), equipped with a load cell that had a maximum capacity of 5 kN. The schematic circuit of the piezoresistive assembly is given in Fig. 2. The samples (height of 4 mm and diameter of 15 mm) were cut from the MRE discoid (at the aforementioned dimensions), and their resistivity was measured at different uniaxial mechanical deformations via the two-probe method. The samples were inserted between gold-plated brass electrodes and compressed gradually from their initial state (F = 3 N) to a maximal compression of 10% (0.4 mm) in steps of 0.05 mm. The deformation rate was set to 5 mm/ min. The samples spent 1 minute at each step of deformation, during which the current–voltage characteristic (from 0 to 10 V) was determined (at laboratory temperature). Conductivity (σ) was determined from said current-voltage dependencies according to the following formula:

$$\sigma = \frac{I}{U}\frac{t}{A} \quad (1)$$

where I represents current, U is voltage, t is thickness decreased by deformation and A is the nominal area of the sample (the area of the electrode).

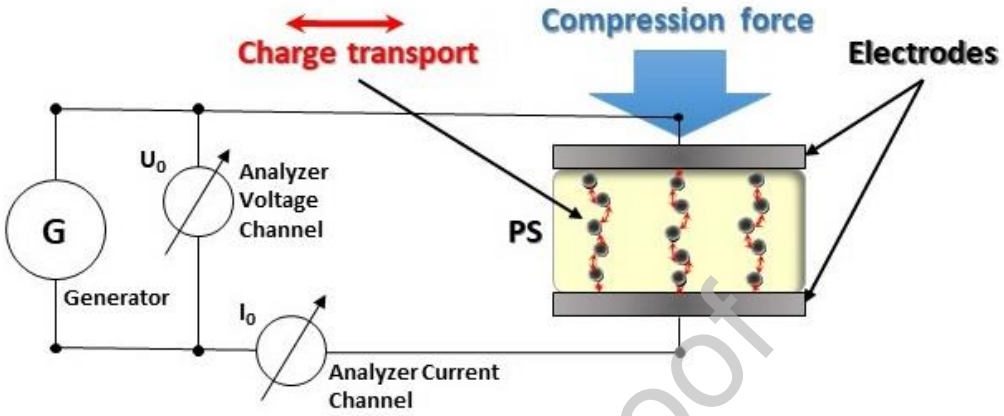

Fig. 2: Image depicting the arrangement of the piezoresistivity test conducted on the MRE-based PSs.

2.3 Optical properties. The particle chain distribution of the MRE-based PSs was studied on a digital microscope (DVM2500, Leica, Switzerland) fitted with a VZ80C adapter controlled by LAS V4.1 software. The samples were illuminated by the upper LED light source. Analysis of the resulting images was carried out in ImageJ software (version 1.52a, National Institutes of Health, USA). The extent of luminous transmittance vertically by the PSs was characterized on a Lovibond RT850i spectrometer (Tintometer Ltd., UK). Measurements were performed in accordance with the ASTM D 1003 standard, with each sample being tested five times. This method encompassed evaluation of specific properties of the planar transparent samples – luminous transmittance and wide-angle-light scattering, in this way providing comprehensive data on the optical properties of the samples.

2.4 Fatigue tests. These were performed on an Instron servo-hydraulic testing machine (Model 8871, USA) equipped with a modified load cell (maximum capacity of 0.4 kN), fitted parallel to the static lower plate (see Fig. 3). Each PS sample was placed between the plates, and pre-conditioned by a force of 3 N (at a ramp rate of 0.01 mm/s). They were

subsequently subjected to a controlled sinusoidal load at a frequency of 1 Hz, with an amplitude of 0.4 mm (a compression deformation of 10%) applied in alignment with the direction of the internal particle structures. A series of the loading cycles occurred, where the number of cycles was set to 10^2, 10^3 and 10^4. After each one, the piezoresistive performance of the PSs was re-evaluated according to the procedure described above. The data was recorded under laboratory conditions.

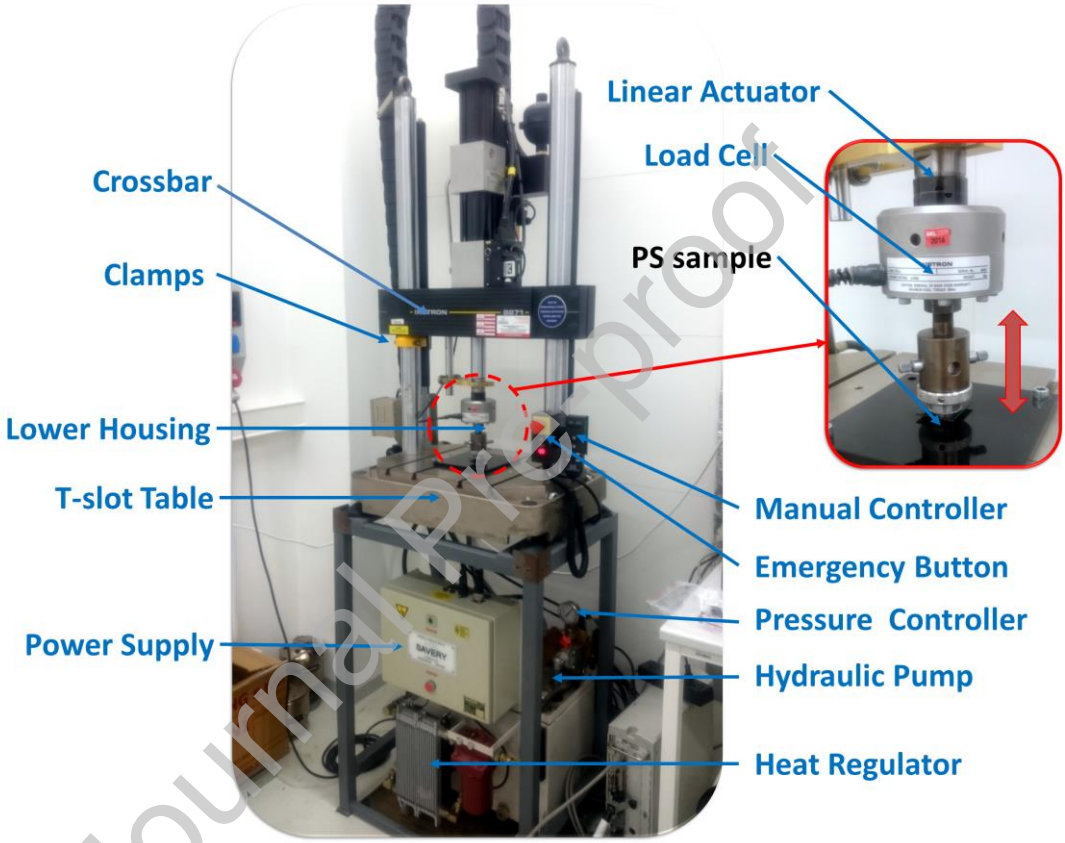

Fig. 3: Apparatus comprising the servo-hydraulic fatigue system for obtaining measurements.

2.5 Microstructure analysis. Scanning electron microscopy (SEM) was conducted on a field-emission SEM device (FEI, Nova NanoSEM 450, Japan) equipped with a low-vacuum detector, under an accelerating voltage of 15 kV, in order to study the effect of cyclic loading on the degradation of the PSs at a microstructural level. Prior to analysis, freeze-fractured samples (liquid N_2) were placed on carbon tape on an aluminium holder

and metallized with a thin layer of gold by a sputtering device (SC7620, Quorum Technologies, UK).

3. Results and discussion

3.1 Piezoresistive characterization. The σ of the MRE-based PSs was measured at various uniaxial deformations. Figure 1a shows the data for a series of the PSs that varied in particle concentration. The non-deformed systems based on a neat matrix exhibited the lowest σ (below 10^{-11} S/cm in ref. [32]), as anticipated. The values for σ gradually rose to 10^{-8} S/cm in line with heightened CI particle concentration. This phenomenon can be explained as a result of the greater amount of particle chains per unit area, these representing the conductive pathways (as described later). Particle concentration also affected the robustness of the particle columns, the majority of which extended throughout the thickness of the sample [25].

Conductive, elastic, particulate composites generally exhibit increase in resistance (a decrease in σ) during elongation due to growth in distance between the metal particles [33]. Contrary behaviour was observed during compression. When the PSs were exposed to the aforementioned step-wise compression, their σ was gradually went up, as highlighted in Fig. 4b. According to the literature [34], such behaviour of σ stems from two main factors. The compression deformation induces increment in the conductive area and, concurrently, the thickness of the polymer membrane between two adjacent particles is progressively reduced. Similar phenomena were recently observed by Shabdin et al.[19] Herein, we were able to quantify increments in σ for the PSs of different CI particle concentrations even without the aid of an additive, e.g. graphite. The results revealed that σ increased 10 fold for PS_1 at the maximum-tested compression, while the enhancement of nearly two orders of magnitude was achieved for PS_7. The resistivity of the PDMS is much higher than that of the CI particles; hence, it was surmised that the resistivity of such a composite primarily depended on the thickness of the PDMS along the conductive path [33]. Based on dielectric

spectroscopy data from the preceding study [23], the charge transport mechanism can be interpreted as variable-range hopping.

At this point, the structural densities of the fabricated PSs were evaluated across the range of concentrations. The density of the PDMS equalled 1.03 g/ cm³ (see the technical data sheet), whereas the value for the CI SL particles was 7.79 g/ cm³ (analysed on a gas pycnometer) [24]. A calculation was performed based on the rule of mixtures under the assumption of an ideal sample without any cavities. As seen in Tab. 1, the PSs became heavier alongside rise in particle concentration, yet increase in density only ever peaked at 6.5%, even though the material possessed conductivity of 100 fold greater. In light of these results, the decision was made to further analyse the optical properties of the MRE-based PSs.

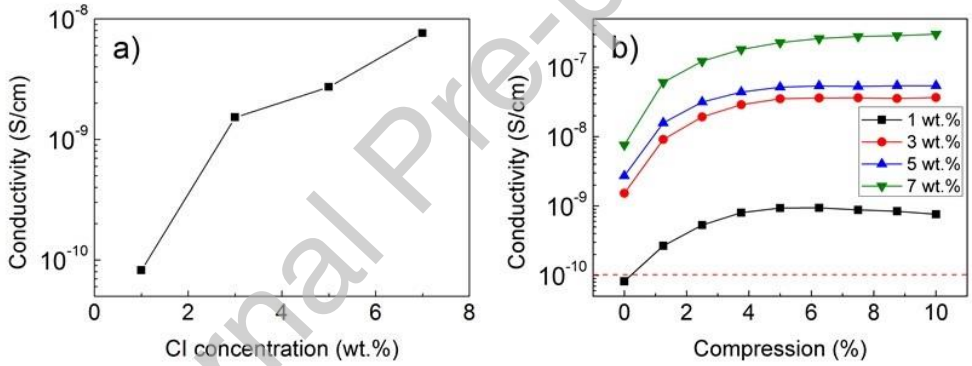

Fig. 4: Dependence of initial conductivity on CI particle concentration (a). The dependencies of conductivity on the relative compression deformation of the MRE-based PSs that varied in content of CI particles (b).

Tab. 1: Relevant parameters for the fabricated PSs.

Sample ID	**CI content (wt.%)**	**CI content (vol.%)**	**Initial σ (S/ cm)**	**Maximum σ (S/ cm)**	**Change in σ (%)**	**Composite density* (g/ cm³)**
PS_0	*0*	*0.00*	*2.5×10^{-16}*	*N/A*	*N/A*	*1.030*

			ref. [32]			
PS_1	1	0.13	8.2×10^{-11}	7.6×10^{-10}	930	1.039
PS_3	3	0.41	1.5×10^{-9}	3.7×10^{-8}	2410	1.058
PS_5	5	0.69	2.7×10^{-9}	5.6×10^{-8}	2550	1.077
PS_7	7	0.99	7.6×10^{-9}	3.02×10^{-7}	3970	1.097

*based on the rule of mixtures calculation

3.2 Optical properties. Applying conductive additives, such as graphite, can increase the σ of composites [19] but it simultaneously increments the degree of opacity, which might prove a limiting factor for certain applications. It is known that composite materials of limited concentration preserve luminous transmittance along the vertical axis, since they possess a suitable arrangement of particle distribution and a transparent matrix [25]. Images of the tops of the PSs containing different CI particle concentrations are displayed in Fig. 5. As shown, the particle chains were relatively well separated and spaced, indicating the external magnetic field (340 mT) had been sufficient to overcome the viscous forces of the liquid-state PDMS and facilitate vertical arrangement of the CI particles. In the case of PS_7, equilibrium was reached for the particles in forming particle chains; although the viscosity of the liquid-state mixture had increased, light was able to penetrate this PS and lend it transparency.

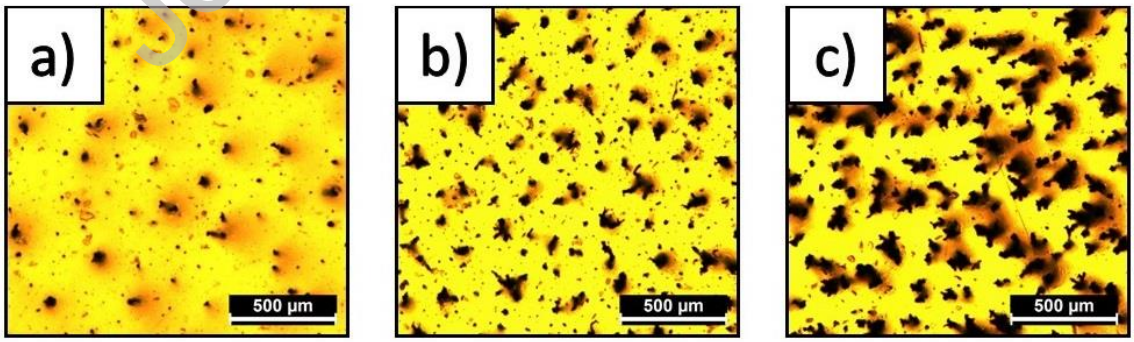

Fig. 5: Optical micrographs showing the top views of the MRE-based PSs of 1, 5, and 7 wt.% (a–c) CI particle concentrations; the thickness of the samples was 4.01±0.10 mm.

Average inter-columnar spacing, Y, can be determined via a structural model that assumes the ideal triangular arrangement of particle columns according to the equation [25]:

$$Y = \sqrt{\frac{D^2}{1.65x}} \qquad (2)$$

where D is particle diameter (9 μm) and x stands for the volume fraction of the particles (Tab. 1). With adherence to the x parameter, the calculated Y values for the studied systems were 198, 113, 87 and 71 μm, confirming the assumption of increase in the concentration-dependent number of particle columns per unit area. The theoretical values for Y were further compared with those extracted from the original images; this required several steps (see Fig. 6). The objects of interest, i.e. the particle columns, were identified by carrying out binarization (Fig. 6b). Since boundaries of particle clusters possess sharp contours, contrast enhancement was not necessary [35]. Afterwards, the image was smoothed out and inverted to easily extract the Y values (Fig. 6c).

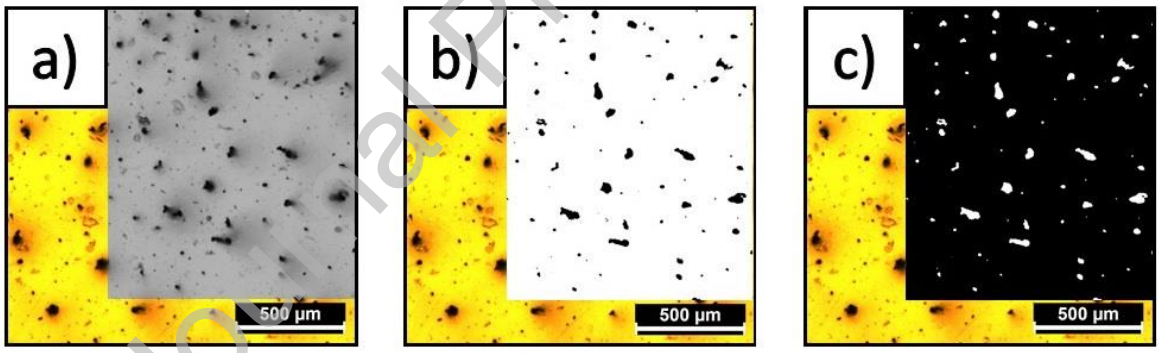

Fig. 6: Example of image analysis of PS_1, showing the greyscale (a), binarized (b) and smoothed/ inverted (c) regions.

Employing such treated images, Y values were quantified as reaching the following values: 156±48.8, 120±37.8, 112±23.0 and 98±25.6 μm. In general, the average values extracted followed the expected trends, although notable standard deviations indicated that imperfections existed in inter-columnar spacing (see Fig. 7). PSs of higher concentrations (PS_5 and PS_7) presented Y values that were slightly higher than the theoretical ones;

potentially a consequence of incomplete particle alignment due to increase in the viscosity of liquid-state PDMS [36]. The possible inhomogeneity of the applied magnetic field and high inter-particle forces could have constituted factors that caused imperfections in particle spacing. Finally, optical micro-observations were conducted throughout the thickness of the PSs (ca 4 mm), thereby magnifying possible aggregates stacked along the particle chains.

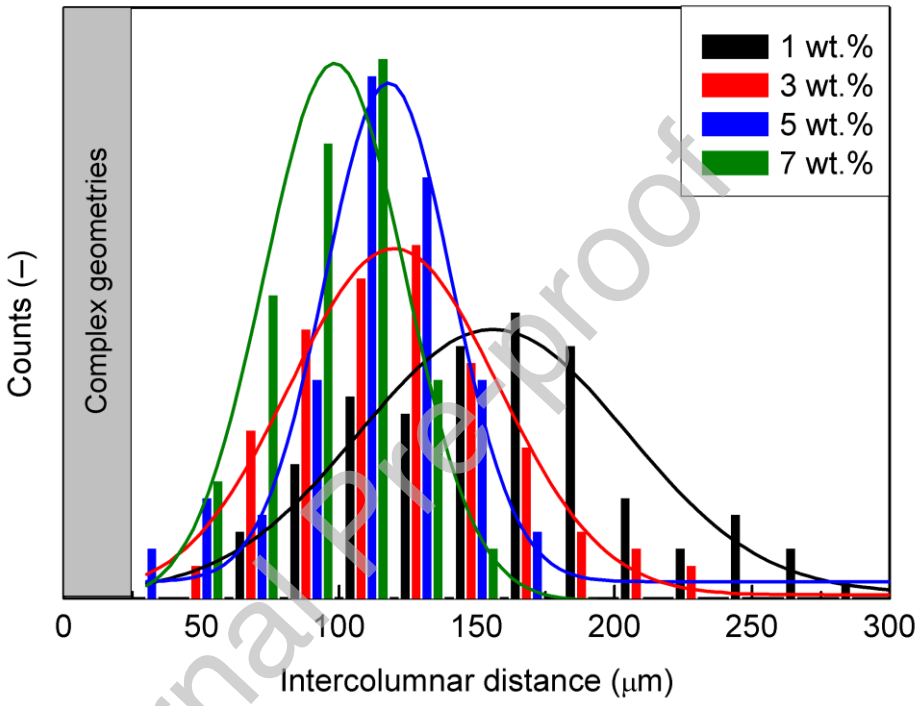

Fig. 7: Distribution of inter-columnar distances for the MRE-based PSs of different CI particle concentration.

Luminous transmittance is a measure of the amount of light that passes through a material, which is of importance in electro-optics. Figure 8 displays the total transmittance of neat PDMS and the PSs along the particle chains plotted against CI particle content. Transmittance formalism dictates that description of the integral properties of a material is achieved by a single value for the entire spectral range. This simplifies comparison of optical properties for a breadth of materials. In this context, neat PDMS exhibited high transparency, in excess of 86%. Total transmittance dropped after embedding the CI, most

likely due to an altered refractive index of strained PDMS in the vicinity of the particles [25]. In parallel with increase in the content of CI, transmittance diminished almost linearly (R^2=0.996). By extrapolating the data, no transparency could be expected at around 16 wt.%. Nevertheless, the transmittance of moderately concentrated PSs (3–5 wt.%) would still make them suitable for optical applications such as touch-sensitive screens [25]. Although these optical properties have been observed to worsen depending on the angle between the composite and incoming light [25], they could not be achieved by self-segregated PS systems [37] or highly-filled (60 wt.%) MRE-based PSs [26].

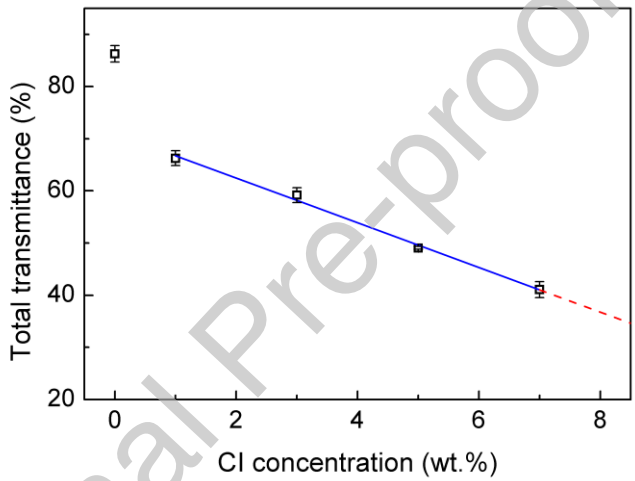

Fig. 8: Dependence of total transmittance on CI particle concentration for the MRE-based PSs. The solid line represents linear fitting, while the dashes denote the extrapolated sequence.

3.2 Fatigue test configuration. PSs predominantly fulfil the function of monitoring in long-term applications [38]. With this in mind, the PSs underwent the defined fatigue test. Such tests are performed either under stress/ load-control or under strain/ deformation-control, the latter one is usually preferred for rubber and plastic [39]. Figure 9 shows the compressive force (response to the sinusoidal strain) exerted on the MRE-based PSs plotted over time. In order to achieve 10% compression, application of relatively high normal force (over 100 N) was required. For the sake of brevity, results are only given for

PS_1 and PS_7, respectively. In the loading phase, compression force peaked at around 107 N for PS_1, whereas the maximum force equalled 128 N for its PS_7 analogue (Fig. 9, insets). This revealed a slight stiffening effect of the inorganic filler, i.e. the CI particles [40]. In the unloading phase, such force returned close-to-zero following removal of the strain input. This suggests that the structure of the PSs recovered well, despite the viscoelastic nature of the PDMS [9]. As for the outcome induced by the number of loads, response to force was relatively stable after few cycles. A similar phenomenon was recently observed by Zheng et al.[38] in research on PDMS-based sensors with various carbonaceous fillers. This behaviour can be attributed to two factors – re-arrangement of the conductive CI particle chains and the motion of polymer macromolecules upon cyclic compression, where the potential exists to proceed to equilibrium [38]. However, description is given later of gradual decrease in σ manifested at higher loading cycles (over 10^3). This explains why a state of equilibrium was not reached, despite the maximal force was almost constant (Fig. 9c). The possible cause of this phenomenon cannot be restricted to a single parameter, as several factors have to be considered, including fatigue-induced migration of the CI particles, heterogeneities in the cross-linking points and change in particle/ matrix interactions [41].

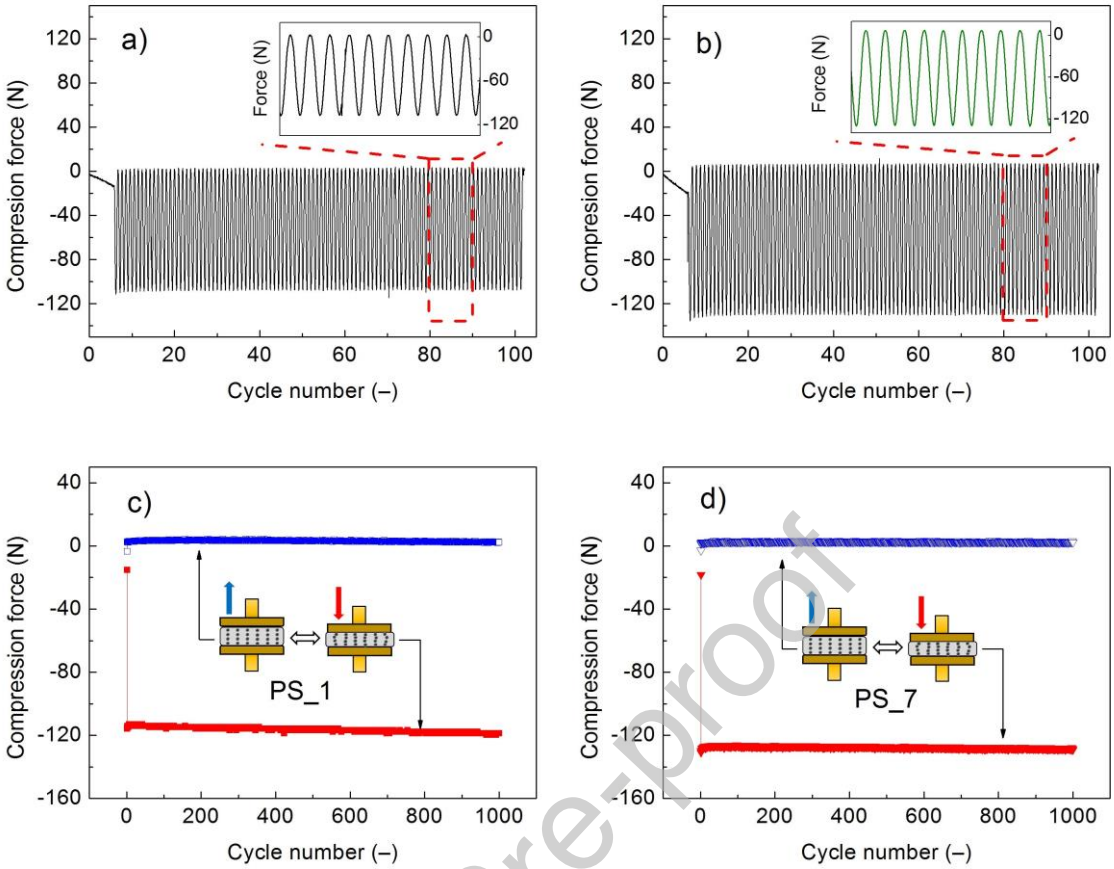

Fig. 9: Dependencies of compression force on the number of cycles (i.e. time represented as frequency equalled 1 Hz) for the PS_1 (a) and PS_7 (b); the inset figures magnify data in the representative regions of the fatigue test. The envelopes of maximum (red) and minimum (blue) force recorded during the fatigue tests for the PS_1 (c), and PS_7 (d).

3.2.1 Effect of cyclic loading on piezoresistivity. Only a few papers in the literature have reported on the effect of fatigue on the piezoresistivity of MRE-based PSs. In an attempt to address this we recorded conductivity–compression curves after 10^2, 10^3 and 10^4 loading cycles, as illustrated in Fig. 10a, b. The contours of the σ curves and their concentration trends remained intact, although σ values gradually decreased alongside rise in the number of loading cycles. The data gathered after 10^4 cycles were not considered, since σ dropped significantly below $< 10^{-10}$ S/cm regardless of CI particle concentration, thus these PSs were considered non-conductors (data not shown). Figure 10c illustrates the overall σ/σ_0 ratio, where σ_0 denotes the conductivity of the freshly prepared composite. This parameter

was calculated as the mean value of the relative conductivities under each stage of compression. The overall σ/σ_0 ratio was notably dependent on CI particle concentration. For the PSs of low concentration (up to 3 wt.%) σ/σ_0 varied little after 10^2 loading cycles, compared to the initial states determined, while decreases of up to 40% were observed for analogues of higher concentrations. This trend resembled the situation after 10^3 cycles, however, the σ/σ_0 parameter was much lower, indicating only residual conductivity. This examination suggests that the amount of CI particle chains, represented by particle concentration, constitutes the key factor involved in the ageing of the PSs (Fig. 10c). Other factors may also have been connected with changes in aspects such as PDMS cross-link density and particle/matrix interactions. In order to evaluate these hypotheses, we performed detailed SEM analysis of freeze-fractured samples.

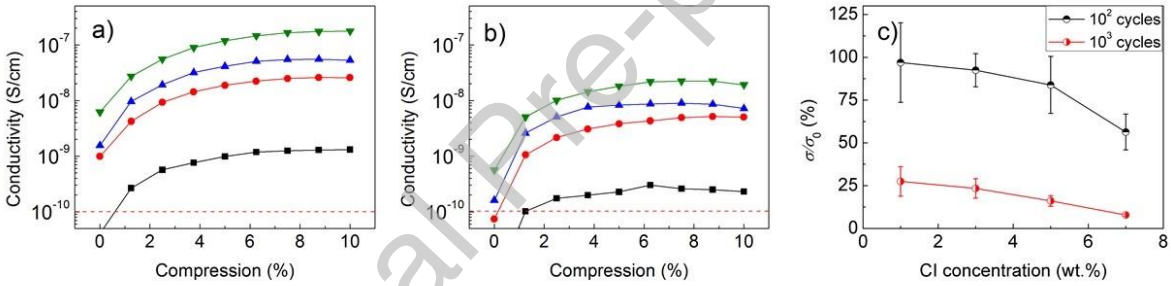

Fig. 10: Dependencies of σ on the relative-compression deformation of the MRE-based PSs with different CI particle content (squares, circles, upward triangles, downward triangles; 1–7 wt.%) after 10^2 (a) and 10^3 (b) loading cycles. The relative σ of the PSs after fatigue tests as a function of CI particle concentration (c).

3.3 Constitutive model of piezoresistance. In order to predict the sensing behaviour of electrically conductive composites, Zhang et al.[42] developed a model based on tunnelling theory, given by the following equation:

$$\frac{R}{R_0} = \left(1 - \frac{\sigma_A}{E}\right) exp\left\{-\gamma D\left[\left(\frac{\pi}{6}\right)^{\frac{1}{3}} \theta^{\frac{-1}{3}} - 1\right]\frac{\sigma}{E}\right\} \quad (3)$$

where R/R_0 denotes relative resistance (R represents resistance upon exerting pressure and R_0 is the original zero-pressure resistance of the sample); σ_A is the applied mechanical stress in sample area A; E stands for the elastic modulus of the matrix; D is the average particle diameter; and θ is the particle volume fraction. The γ is the quantum tunnelling term that contains information about potential barrier height between the conductive filler and matrix material [29, 43]. The exponential form of the model reflects the physical reality of tunnelling current, which decays exponentially as tunnelling distance increases. The term inside the exponent describes changes in inter-particle distances for the particles arranged in a simple cubic lattice [29]. This form of model describes the piezoresistance of composites based on linearly elastic polymer matrices with spherical, uniformly distributed particles. However, it fails to precisely correlate with highly non-linear materials, e.g. elastomers with high aspect ratio fillers such as graphite and carbon nanotubes, or with particles which create complex conductive networks like carbon black [44]. Herein, the latter piezoresistance response was expected, in consideration of the characteristics of the PDMS and anisotropic arrangement of the CI particles.

The analytical form of the piezoresistance model can be generalized with the following form:

$$\frac{R}{R_0} = \left(1 - \frac{\sigma_A}{E}\right) exp\left[-C\left(\frac{\sigma_A}{E}\right)\right] \quad (4)$$

which shares the same parameters defined above, while the constant C replaces the terms for tunnelling factor, filler geometry and filler arrangement. As is apparent from the equation, inter-particle spacing and R depends on strain, assumed to follow Hooke's law. In the context of this simple assumption, the model has not always correlated well with experimental data. As a consequence, Rizvi et al.[29] modified the strain function in the model to adhere to power-law proportionality. The resultant equation is written as:

$$\frac{R}{R_0} = \left[1 - \left(\frac{\sigma_A}{E}\right)^{\frac{1}{n}}\right] exp\left[-C\left(\frac{\sigma_A}{E}\right)^{\frac{1}{n}}\right] \quad (5)$$

where C, E and n are fitting parameters. Such a model seems to possess the necessary attributes to determine the piezoresistivity of the anisotropic MRE-based PSs described herein.

Figure 11 shows R/R_0 values as a function of applied mechanical stress for the MRE-based PSs embedded with different amounts of CI particles. The R/R_0 dependencies followed the trend of decrease due to strain-induced drop in the average distance between the particle conductive pathways, separated by thin segments of neat PDMS (as proven later by SEM analysis). These dependencies had a tendency to level off once the maximal number of microstructural conductive pathways had been established. Before interpretation of the data is given, it worth noting that the R/R_0 dependence for PS_1 exhibited a trend of increase after exceeding a certain level of σ_A (ca 3 kPa), potentially indicating breakdown of the conductive pathways and consequential decrease in tunnelling current due to severe compression deformation. For this reason the piezoresistive model was applied only to the monotonously decreasing part of the R/R_0 curve.

A method for evaluating the sensitivity of piezoresistance is to compare the minimum value of R/R_0 for samples [29]. In this context, the sensitivity to mechanical load of the MRE-based PSs increased in line with CI particle concentration (Fig. 11a), a phenomenon closely associated with the greater number of conductive pathways created in the more concentrated PSs. The sample denoted PS_1 exhibited an R/R_0 10-fold lower upon stress of 2 kPa, while this parameter decreased by almost 100 times for PS_7 under the same pressure. This result demonstrates the remarkable sensing capabilities of the anisotropic MRE-based PSs. For the sake of comparison, the PDMS- and PE-based composites filled with randomly distributed multi-wall carbon nanotubes (up to 6 wt.%) required much higher application of stress (above 0.2 MPa) to achieve low R/R_0, while certain composites failed to even register such R/R_0 values [29].

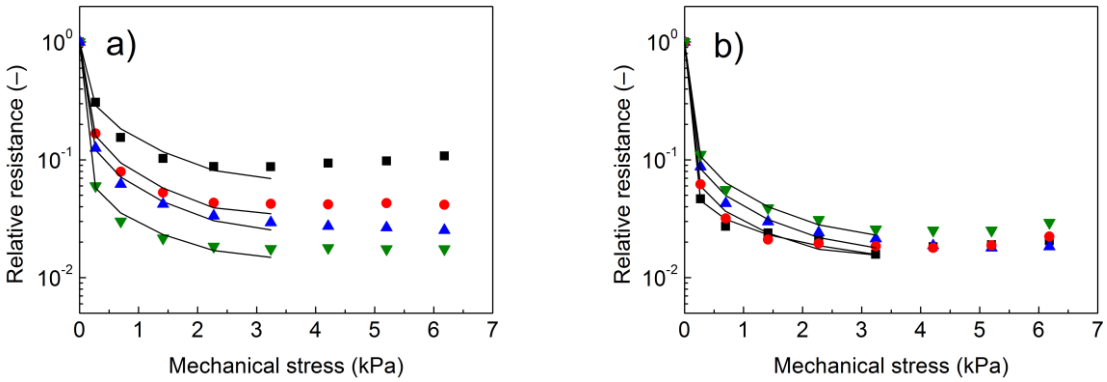

Fig. 11: Dependencies of R/R_0 on applied mechanical stress for the MRE-based PSs with different CI particle content (squares, circles, upward triangles, downward triangles; 1–7 wt.%) after fabrication (a) and after 10^3 (b) loading cycles; the solid lines denote the fit of the model.

Accuracy was also gauged for the fit of the modified piezoresistance model. As seen in Fig. 11, the applied model provided satisfactory description of data and reasonably high correlation coefficients (R^2). Numerical results for fitting coefficient values are presented in Tab. 2. Interestingly, the analytical solution of the model was found with the E parameter almost exactly matching the compression modulus of PDMS [45]. The computed C values showed decrease alongside rise in CI particle concentration, thus they followed the pattern for piezoresistance sensitivity expressed as $(R/R_0)_{min}$. After performing 10^3 loading cycles, the PSs exhibited different trends for R/R_0 dependencies (Fig. 11b), primarily since the MRE-based PSs of higher CI concentration were more susceptible to ageing (Fig. 10c). Based on these findings, the PSs exhibited seemingly higher R/R_0 sensitivity compared to the original samples (Tab. 2). However, the primary cause for said sensitivity is perceived as their higher initial resistance [29].

Tab. 2: Material parameters of the compressive piezoresistance model for the MRE-based PSs after fabrication and 10^3 loading cycles.

After fabrication

Sample ID	$(R/R_0)_{min}$	E (MPa)	n	C	R^2
PS_1	*0.087*	*147.1*	*3.01*	*98.5*	*0.969*
PS_3	*0.041*	*148.0*	*3.73*	*62.3*	*0.978*
PS_5	*0.025*	*149.5*	*4.22*	*47.4*	*0.989*
PS_7	*0.017*	*150.8*	*5.99*	*24.9*	*0.978*
After 10^3 cycles					
Sample ID	$(R/R_0)_{min}$	E (MPa)	n	C	R^2
PS_1	*0.016*	*152.7*	*8.60*	*13.3*	*0.978*
PS_3	*0.018*	*151.3*	*5.88*	*25.7*	*0.977*
PS_5	*0.018*	*149.6*	*4.89*	*36.0*	*0.985*
PS_7	*0.025*	*149.5*	*4.53*	*40.4*	*0.988*

3.3 Evaluation of microstructure. As the fatigue-induced decrease in σ was clearly dependent on CI particle concentration (Fig. 10c), the most significant microstructural changes were expected to appear in PS_7, hence this sample was subjected to SEM analysis. Fracturing was deliberately carried out along the particle chains, i.e. the compression axis. As seen in Fig. 12, the CI particles were perfectly organized, almost in chains of single particle width even at a microstructural level. After 10^4 loading cycles, however, particle alignment was relatively distorted, demonstrating increased inter-particle distances were present, which prevented formation of conductive pathways and the existence of tunnelling current. PDMS typically exhibits a relatively smooth fracture surface [46], which applied for the original sample herein. However, the morphology of fatigue fracture revealed layered patterns perpendicular to the compression plane. These local (Fig. 12b), and interfacial (Fig. 12d) inhomogeneities might have been caused by stress concentration and irreversible changes in the PDMS matrix. Moreover, fatigue-induced variation in the particle/matrix interface was also apparent. As indicated by red dashes, the cyclic loading

induced debonding of the CI particles from the PDMS and the appearance of small cavities around individual particles. This phenomenon indicates weak interfacial compatibility [47] and most likely constitutes the main factor behind the dramatic decrease in σ, as discussed in the following section.

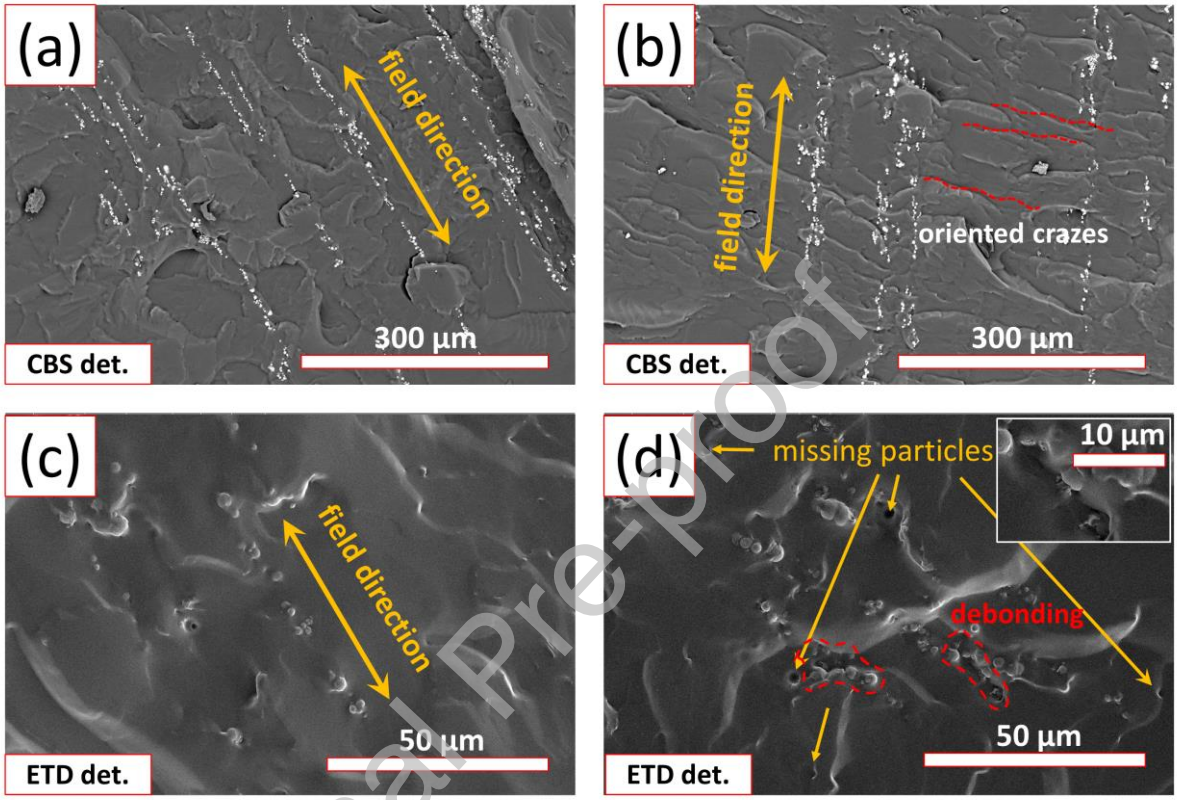

Fig. 12: SEM images and magnified pictures of the freeze-fractured PS_7 after fabrication (a, c) and 10^4 (b, d) loading cycles.

3.4 Discussion. The data from the displacement-controlled fatigue tests revealed that the σ of the MRE-based PSs markedly decreased after the point of 10^3 cycles, highlighting the low resilience of the PSs to the experimental conditions imposed. This may be attributable to several factors including: (i) destruction of the PDMS polymer network upon the non-linear compression deformations performed [41]; (ii) rupture of CI/PDMS covalent bonds, a likely occurrence in these systems [9], which consequently increased inter-particle distances and diminished the conductivity of the composite. In light of this, an operating mode based on minor deformations could help extend the service life of such PSs. This

hypothesis is supported by the fact that σ already plateaued under compression of less than 6% (Fig. 4b), an aspect which also applied to high R/R_0 sensitivity (Fig. 11). Such a low magnitude of deformation could be a limiting factor in the detection of certain signals, such as human motion [48], although it shows promise for tactile applications [25]. Notably, the concept presented for fabricating PSs herein is simple and provides samples with high reproducibility, thereby overcoming typical challenges faced when developing sensors.

A further enhancement is possible, comprising modification of CI particles with substances that possess a great affinity for non-polar matrices, such as organosilanes [49, 50]; this appears to be a promising way to produce highly resilient composites. For instance, Al Akoum et al.[51] investigated the positive effects of the degree of silanization on the adsorption of PDMS, while An et al.[52] reported on the enhanced affinity of silane-treated CI particles for natural rubber, compared to unmodified analogues. Further research is clearly required to explore the feasibility of the indicated approaches.

4. Conclusions

In conclusion, we successfully fabricated PDMS-based PSs conceptualized as anisotropic MREs with 1–7 wt.% CI particle concentration. These flexible PSs exhibited a dramatically lower percolation threshold in comparison with their isotropic analogues, since the organized particle structures served as pathways for transport of electric charge, most probably via a variable-range hopping mechanism. Due to the low CI content, the samples exhibited negligible structural density, not exceeding 1.097 g/cm^3, and high transmittance of light vertically, both enormously beneficial properties for engineering. Compressing the PSs led to gradual rise in σ by up to 2 orders of magnitude (3.02×10^{-7} S/cm) due to decrease in the thickness of the PDMS membrane between the CI particles. Their sensitivity in terms of R/R_0 was remarkably high compared to isotropic PSs found elsewhere in the literature. In the strain-control fatigue test, force peaked at around 107 N in order to compress PS_1 by 10%, whereas PS_7 required a force of 128 N to achieve the

same compression. Following the number of loads carried out, compression force was relatively stabilized after a few cycles, attributed to the state of equilibrium between the re-arrangement of the CI particle chains and the motion of the PDMS macromolecules. However, values for σ gradually dropped, decreasing in line with performance of each subsequent loading cycle. The σ/σ_0 ratio was notably dependent on the content of CI particles, demonstrating the PSs of low concentration (up to 3 wt.%) were more resilient. After 10^4 cycles, σ dropped significantly below the point of 10^{-10} S/cm, thus the PSs were considered non-conductors. SEM analysis revealed the presence of fatigue-induced microstructural inhomogeneities, stemming from stress concentration and irreversible changes in the PSs. Debonding by the CI particles further indicated weak interfacial compatibility. Thus, surface treatment of CI particles, such as by silanization, could enhance particle/matrix affinity, bringing about highly durable PSs. We also suggest applying a lower compression amplitude, of less than 6%, due to the saturation of σ observed, in order to limit how the PSs age.

Declaration of interest: *none*

Acknowledgements

The authors wish to thank the Czech Science Foundation (17-24730S) for its financial support. This work was also supported by the Ministry of Education, Youth and Sports of the Czech Republic – Programme NPU I (LO1504).

References

[1] Fiorillo AS, Critello CD, Pullano SA. Theory, technology and applications of piezoresistive sensors: A review. Sens Actuators A **2018***; 281: 156-75, doi:10.1016/j.sna.2018.07.006.*

[2] Regtien PPL. Resistive sensors. In: Sensors for mechatronics, Elsevier Science Bv: Amsterdam, 2012; 57-100, doi:10.1016/b978-0-12-391497-2.00004-2.

[3] Pham GT, Park YB, Liang Z, Zhang C, Wang B. Processing and modeling of conductive thermoplastic/ carbon nanotube films for strain sensing. Composites, Part B **2008***; 39: 209-16, doi:10.1016/ j.compositesb.2007.02.024.*

[4] Shang SY, Yue YJ, Wang XE. Piezoresistive strain sensing of carbon black / silicone composites above percolation threshold. Rev Sci Instrum **2016***; 87: 123910, doi:10.1063/ 1.4973274.*

[5] Zhang W, Suhr J, Koratkar N. Carbon nanotube/ polycarbonate composites as multifunctional strain sensors. J Nanosci Nanotechnol **2006***; 6: 960-4, doi:10.1166/ jnn.2006.171.*

[6] Rinaldi A, Tamburrano A, Fortunato M, Sarto MS. A flexible and highly sensitive pressure sensor based on a PDMS foam coated with graphene nanoplatelets. Sensors **2016***; 16: 2148, doi:10.3390/ s16122148.*

[7] Ye XL, Yuan Z, Tai HL, Li WZ, Du XS, Jiang YD. A wearable and highly sensitive strain sensor based on a polyethylenimine-rGO layered nanocomposite thin film. J Mater Chem C **2017***; 5: 7746-52, doi:10.1039/ c7tc01872j.*

[8] Bica I, Anitas EM, Bunoiu M, Vatzulik B, Juganaru I. Hybrid magnetorheological elastomer: Influence of magnetic field and compression pressure on its electrical conductivity. J Ind Eng Chem **2014***; 20: 3994-9, doi:10.1016/ j.jiec.2013.12.102.*

[9] Cvek M, Mrlik M, Ilcikova M, Mosnacek J, Munster L, Pavlinek V. Synthesis of silicone elastomers containing silyl-based polymer grafted carbonyl iron particles: An efficient way to improve magnetorheological, damping, and sensing performances. Macromolecules **2017***; 50: 2189-200, doi:10.1021/ acs.macromo1.6b02041.*

[10] Cvek M, Kracalik M, Sedlacik M, Mrlik M, Sedlarik V. Reprocessing of injection-molded magnetorheological elastomers based on TPE matrix. Composites, Part B **2019***; 172: 253-61, doi:10.1016/ j.compositesb.2019.05.090.*

[11] Li YC, Li JC, Li WH. Du HP. A state-of-the-art review on magnetorheological elastomer devices. Smart Mater Struct **2014***; 23: 123001, doi:10.1088/ 0964-1726/ 23/ 12/ 123001.*

[12] Bica I. Influence of the transverse magnetic field intensity upon the electric resistance of the magnetorheological elastomer containing graphite microparticles. Mater Lett **2009***; 63: 2230-2, doi:10.1016/ j.matlet.2009.07.032.*

[13] Cvek M, Mrlik M, Sevcik J, Sedlacik M. Tailoring performance, damping, and surface properties of magnetorheological elastomers via particle-grafting technology. Polymers **2018***; 10: 1411, doi:10.3390/ polym10121411.*

[14] Moucka R, Sedlacik M, Kutalkova E. Magnetorheological elastomers: Electric properties versus microstructure. AIP Conf Proc **2018***; 2022: 020017, doi:10.1063/ 1.5060697.*

[15] Karasek L, Meissner B, Asai S, Sumita M. Percolation concept: Polymer-filler gel formation, electrical conductivity and dynamic electrical properties of carbon-black-filled rubbers. Polym J **1996***; 28: 121-6, doi:10.1295/ polymj.28.121.*

[16] Kchit N, Bossis G. Electrical resistivity mechanism in magnetorheological elastomer. J Phys D: Appl Phys **2009***; 42: 105505, doi:10.1088/ 0022-3727/ 42/ 10/ 105505.*

[17] Bica I. The influence of the magnetic field on the elastic properties of anisotropic magnetorheological elastomers. J Ind Eng Chem **2012***; 18: 1666-9, doi:10.1016/ j.jiec.2012.03.006.*

[18] Wang XJ, Gordaninejad F, Calgar M, Liu YM, Sutrisno J, Fuchs A. Sensing behavior of magnetorheological elastomers. J Mech Des **2009***; 131: 091004, doi:10.1115/ 1.3160316.*

[19] Shabdin MK, Abdul Rahman MA, Mazlan SA, Ubaidillah U, Hapipi NM, Adiputra D, Abdul Aziz SA, Bahiuddin I, Choi SB. Material characterizations of Gr-based

magnetorheological elastomer for possible sensor applications: Rheological and resistivity properties. Materials **2019***; 12: 391: doi:10.3390/ ma12030391.*

[20] Ginder JM, Nichols ME, Elie LD, Tardiff JL. Magnetorheological elastomers: Properties and applications. Proc. SPIE 3675, Smart Struct Mater 1999: Smart Mater Technol **1999***; 3675: 131-8, doi:10.1117/ 12.352787.*

[21] Li R, Sun LZ. Viscoelastic responses of silicone-rubber-based magnetorheological elastomers under compressive and shear loadings. J Eng Mater Technol **2013***; 135: 021008, doi:10.1115/ 1.4023839.*

[22] Boczkowska A, Awietjan SF, Wroblewski R. Microstructure-property relationships of urethane magnetorheological elastomers. Smart Mater Struct **2007***; 16: 1924-30, doi:10.1088/ 0964-1726/ 16/ 5/ 049.*

[23] Moucka R, Sedlacik M, Cvek M. Dielectric properties of magnetorheological elastomers with different microstructure. Appl Phys Lett **2018***; 112: 122901, doi:10.1063/ 1.5021750.*

[24] Cvek M, Moucka R, Sedlacik M, Babayan V, Pavlinek V. Enhancement of radio-absorbing properties and thermal conductivity of polysiloxane-based magnetorheological elastomers by the alignment of filler particles. Smart Mater Struct **2017***; 26: 095005, doi:10.1088/ 1361-665X/ aa7ef6.*

[25] Jin S, Tiefel TH, Wolfe R, Sherwood RC, Mottine JJ. Optically transparent, electrically conductive composite medium. Science **1992***; 255: 446-8, doi:10.1126/ science.255.5043.446.*

[26] Zhang W, Gong XL, Jiang WQ, Fan YC. Investigation of the durability of anisotropic magnetorheological elastomers based on mixed rubber. Smart Mater Struct **2010***; 19: 085008, doi:10.1088/ 0964-1726/ 19/ 8/ 085008.*

[27] Wang Y, Xuan SH, Ge L, Wen QQ, Gong XL. Conductive magnetorheological elastomer: Fatigue dependent impedance-mechanic coupling properties. Smart Mater Struct **2017***; 26: 015004, doi:10.1088/ 0964-1726/ 26/ 1/ 015004.*

[28] Schumann M, Morich J, Kaufhold T, Bohm V, Zimmermann K, Odenbach S. A mechanical characterisation on multiple timescales of electroconductive magnetorheological elastomers. J Magn Magn Mater **2018***; 453: 198-205, doi:10.1016/ j.jmmm.2018.01.029.*

[29] Rizvi R, Cochrane B, Biddiss E, Naguib H. Piezoresistance characterization of poly(dimethyl-siloxane) and poly(ethylene) carbon nanotube composites. Smart Mater Struct **2011***; 20: 094003, doi:10.1088/ 0964-1726/ 20/ 9/ 094003.*

[30] Moradi-Dastjerdi R, Behdinan K. Stability analysis of multifunctional smart sandwich plates with graphene nanocomposite and porous layers. Int J Mech Sci **2020***; 167: 105283, doi:10.1016/ j.ijmecsci.2019.105283.*

[31] Bodaghi M, Liao WH. 4D printed tunable mechanical metamaterials with shape memory operations. Smart Mater Struct **2019***; 28: 045019, doi:10.1088/ 1361-665X/ ab0b6b.*

[32] Jin GJ, Uddin MJ, Shim JS. Biomimetic cilia-patterned rubber electrode using ultra conductive polydimethylsiloxane. Adv Funct Mater **2018***; 28: 1804351, doi:10.1002/ adfm.201804351.*

[33] Yun GL, Tang SY, Sun SS, Yuan D, Zhao QB, Deng L, Yan S, Du HP, Dickey MD, Li WH. Liquid metal-filled magnetorheological elastomer with positive piezoconductivity. Nat Commun **2019***; 10: 1300, doi:10.1038/ s41467-019-09325-4.*

[34] Tian TF, Li WH, Deng YM. Sensing capabilities of graphite based MR elastomers. Smart Mater Struct **2011***; 20: 025022, doi:10.1088/ 0964-1726/ 20/ 2/ 025022.*

[35] Dominguez-Garcia P, Rubio MA. JChainsAnalyser: an ImageJ-based stand-alone application for the study of magneto-rheological fluids. Comput Phys Commun **2009***; 180: 1956-60, doi:10.1016/ j.cpc.2009.04.016.*

[36] Khairi MHA, Fatah AYA, Mazlan SA, Ubaidillah U, Nordin NA, Ismail NIN, Choi SB, Aziz SAA. Enhancement of particle alignment using silicone oil plasticizer and its effects on the field-dependent properties of magnetorheological elastomers. Int J Mol Sci **2019***; 20: 4085, doi:10.3390/ ijms20174085.*

[37] Costa P, Oliveira J, Horta-Romaris L, Abad MJ, Moreira JA, Zapirain I, Aguado M, Galvan S, Lanceros-Mendez S. Piezoresistive polymer blends for electromechanical sensor applications. Compos Sci Technol **2018***; 168: 353-62, doi:10.1016/ j.compscitech.2018.10.022.*

[38] Zheng YJ, Li YL, Li ZY, Wang YL, Dai K, Zheng GQ, Liu CT, Shen CY. The effect of filler dimensionality on the electromechanical performance of polydimethylsiloxane based conductive nanocomposites for flexible strain sensors. Compos Sci Technol **2017***; 139: 64-73, doi:10.1016/ j.compscitech.2016.12.014.*

[39] Tao G, Xia ZH. A non-contact real-time strain measurement and control system for multiaxial cyclic/ fatigue tests of polymer materials by digital image correlation method. Polym Test **2005***; 24: 844-55, doi:10.1016/ j.polymertesting.2005.06.013.*

[40] Fu SY, Feng XQ, Lauke B, Mai YW. Effects of particle size, particle/ matrix interface adhesion and particle loading on mechanical properties of particulate-polymer composites. Composites, Part B **2008***; 39: 933-61, doi:10.1016/ j.compositesb.2008.01.002.*

[41] Kroth T, Lellinger D, Alig I, Wallmichrath M. Combination of cyclic fatigue testing and materials characterisation to investigate ageing of elastomers. Int Polym Sci Technol **2017***; 44: 1-8, doi:10.1177/ 0307174X1704400401.*

[42] Zhang XW, Pan Y, Zheng Q, Yi XS. Time dependence of piezoresistance for the conductor-filled polymer composites. J Polym Sci, Part B: Polym Phys **2000***; 38: 2739-49, doi:10.1002/ 1099-0488(20001101)38:21<2739::AID-POLB40>3.0.CO;2-O.*

[43] Liu H, Li YL, Dai K, Zheng GQ, Liu CT, Shen CY, Yan XG, Guo J, Guo Z. Electrically conductive thermoplastic elastomer nanocomposites at ultralow graphene

loading levels for strain sensor applications. J Mater Chem C **2016***; 4: 157-66, doi:10.1039/ C5TC02751A.*

[44] Wang LH, Ding TH, Wang P. Influence of carbon black concentration on piezoresistivity for carbon-black-filled silicone rubber composite. Carbon **2009***; 47: 3151-7, doi:10.1016/ j.carbon.2009.06.050.*

[45] Johnston ID, McCluskey DK, Tan CKL, Tracey MC. Mechanical characterization of bulk Sylgard 184 for microfluidics and microengineering. J Micromech Microeng **2014***; 24: 035017, doi:10.1088/ 0960-1317/ 24/ 3/ 035017.*

[46] Huang NJ, Zang J, Zhang GD, Guan LZ, Li SN, Zhao L, Tang LC. Efficient interfacial interaction for improving mechanical properties of polydimethylsiloxane nanocomposites filled with low content of graphene oxide nanoribbons. RSC Adv **2017***; 7: 22045-53, doi:10.1039/ c7ra02439h.*

[47] Lapcik L, Manas D, Lapcikova B, Vasina M, Stanek M, Cepe K, Vlcek J, Waters KE, Greenwood RW, Rowson NA. Effect of filler particle shape on plastic-elastic mechanical behavior of high density poly(ethylene)/ mica and poly(ethylene)/ wollastonite composites. Composites, Part B **2018***; 141: 92-9, doi:10.1016/ j.compositesb.2017.12.035.*

[48] Cai L, Song L, Luan PS, Zhang Q, Zhang N, Gao QQ, et al. Super-stretchable, transparent carbon nanotube-based capacitive strain sensors for human motion detection. Sci Rep **2013***; 3: 3048, doi:10.1038/ srep03048.*

[49] Cvek M, Moucka R, Sedlacik M, Pavlinek V. Electromagnetic, magnetorheological and stability properties of polysiloxane elastomers based on silane-modified carbonyl iron particles with enhanced wettability. Smart Mater Struct **2017***; 26: 105003, doi:10.1088/ 1361-665X/ aa85c5.*

[50] Ikaev AM, Mingalyov PG, Lisichkin GV. Chemical modification of iron oxide surface with organosilicon and organophosphorous compounds. Colloid J **2007***; 69: 741-6, doi:10.1134/ s1061933x07060105.*

[51] Al Akoum R, Vaulot C, Schwartz D, Hirn MP, Haidar B. How Silanization of silica particles affects the adsorption of PDMS chains on its surface. J Polym Sci, Part B: Polym Phys **2010***; 48: 2371-8, doi:10.1002/ polb.22130.*

[52] An JS, Kwon SH, Choi HJ, Jung JH, Kim YG. Modified silane-coated carbonyl iron/ natural rubber composite elastomer and its magnetorheological performance. Compos Struct **2017***; 160: 1020-6, doi:10.1016/ j.compstruct.2016.10.128.*

Author Statement

Title: Lightweight, transparent piezoresistive sensors conceptualized as anisotropic magnetorheological elastomers: A durability study

Authors:

Martin Cvek: Conceptualization; Methodology; Validation; Formal analysis; Investigation; Software; Writing – Original Draft; Writing – Review & Editing; Visualization

Erika Kutalkova: Investigation

Robert Moucka: Methodology; Validation; Investigation; Writing – Review & Editing

Pavel Urbanek: Investigation

Michal Sedlacik: Conceptualization; Validation; Writing – Review & Editing; Supervision; Project administration; Funding acquisition